Planetary and Space Science 122 (2016) 101–109

Contents lists available at ScienceDirect

Planetary and Space Science

journal homepage: www.elsevier.com/locate/pss

Thermal behavior of regolith at cold traps on the moon's south pole: Revealed by Chang'E-2 microwave radiometer data

Guangfei Wei [a], Xiongyao Li [a,*], Shijie Wang [b]

[a] Center for Lunar and Planetary Sciences, Institute of Geochemistry, Chinese Academy of Sciences, Guiyang 550081, China
[b] State Key Laboratory of Environmental Geochemistry, Institute of Geochemistry, Chinese Academy of Sciences, Guiyang 550081, China

ARTICLE INFO

Article history:
Received 14 October 2015
Received in revised form
19 January 2016
Accepted 20 January 2016
Available online 26 January 2016

Keywords:
Chang'E
Brightness temperature
Cold traps
Thermal behavior
Moon

ABSTRACT

The long-term stability of water ice at cold traps depends on subsurface temperature and regolith thermophysical properties. Based on Chang'E-2 microwave radiometer data, we have inverted attenuation coefficient, thermal gradient and instantaneous temperature profiles at permanently shaded craters (Cabeus, Haworth and Shoemaker) on the Moon's south pole. The nonuniformity of the inverted attenuation coefficient within the craters reflects the inhomogeneous thermophysical properties of regolith. In addition, thermal gradient decreased significantly from the crater walls to the bottoms, which may be caused by scattered sunlight, internal heat flux and earthshine effect. Considering continuous supplement of water ice (with volumetric fraction 0–10%) at cold traps, it changes subsurface thermophysical properties but has little effect on thermal gradient. We also assumed that abundant ice (10%) mixed with regolith, the inversion results showed that the maximum difference of diurnal temperatures between "wet" and dry regolith were no more than 0.5 K. That is, the effect of water ice on subsurface thermal behavior can be neglected.

1. Introduction

Cold traps at the Moon's south polar region are the most fascinating and important destinations for lunar explorations in search of water and sites for future human colonization. Due to small oblique angle of the Moon's spin axis with respect to ecliptic (1.54°), the plausibility of existence of water ice in cold traps was initially discussed by Watson et al. (1961). Cold traps favorably harbor water ice that originates from occasional comets, water-containing meteorites, and solar-wind-induced iron reduction of regolith; yet ice is lost due to solar wind sputter erosion (Arnold, 1979; Crider and Vondrak, 2002, 2003; Klumov and Berezhnoi, 2002). The processes of deposition and sublimation in these regions have been sustained for nearly 2 Gyr, since the Moon's orbital evolution became stable (Arnold, 1979; Bills and Ray, 1999).

Both radar experiments and neutron spectrometer readings have implied that water ice is concentrated at cold traps in lunar south polar regions (Nozette et al., 1996; Feldman et al., 1998; Mitrofanov et al., 2010). Recently, hydroxyl and water have been founded to focus in polar regions by global scale infrared detection in three separate missions, Cassini (Clark, 2009), Chandrayaan-1 (Pieters et al., 2009) and Deep Impact (Sunshine et al., 2009). In addition, the presence of water ice was confirmed later by impact experiment at Cabeus crater using observations of near-infrared and ultraviolet/visible spectrometers onboard the Lunar Crater Observation and Sensing Satellite (LCROSS) (Colaprete et al., 2010; Schultz et al., 2010).

Indeed, the stability of water ice at cold traps is predominantly controlled by thermal behavior of lunar regolith (e.g., Salvail and Fanale, 1994; Lucey et al., 2004; Schorghofer and Taylor, 2007; Paige et al., 2010b; Siegler et al., 2011; Schorghofer and Aharonson, 2014). Thermal regime within these regions are governed by regolith thermophysical properties, topographically-driven scattered sunlight, surface thermal re-radiation, internal heat flows and earthshine (Paige et al., 2010b; Sefton-Nash et al., 2013; Siegler et al., 2015). Water molecules can also be enhanced in excess of surface concentration by pumping effect due to temperature cycle, and the ice would become thermal immobile once the maximum temperatures dropped below ~100 K (Schorghofer and Aharonson, 2014; Siegler et al., 2015). For the continuous ice delivering and space weathering at cold traps in the Moon's geologic history, thermal behavior of the ice regolith mixture may become complex.

Recently, lunar surface thermal radiation and regolith thermophysical properties are investigated by Diviner Lunar Radiometer Experiment (Diviner) onboard Lunar Reconnaissance Orbiter, especial for lunar south polar regions (Paige et al., 2010b; Vasavada et al., 2012). The Diviner experiment is designed to

* Corresponding author.
E-mail address: lixiongyao@vip.skleg.cn (X. Li).

http://dx.doi.org/10.1016/j.pss.2016.01.013
0032-0633/

observe lunar global thermal environment. It contains two spectral channels for reflected solar radiation (each 0.35–2.8 μm) and seven channels for surface infrared emission (ranging 7.55–400 μm) (Paige et al., 2010a). At a low polar orbit 50 km, Diviner observes lunar surface with spatial resolution of ~200 m and an image swath of 3.4 km. Based on repeat coverage of Diviner observations at polar regions, cryogenic regions are identified and the locations where water ice might be cold trapped are investigated (Paige et al., 2010b). However, for the shallow penetration depth of thermal infrared, regolith thermal behavior and thermophysical properties at greater depths cannot be revealed directly by observed data.

Chang'E-2 (CE-2), China's second lunar probe, was launched on October 1, 2010. Microwave radiometer (MRM) onboard CE-2 is the same as its predecessor onboard Chang'E-1 (CE-1) which has four channels: 3.0, 7.8, 19.35, and 37 GHz (Fang and Fa, 2014). For the lower altitude of CE-2, approximately 100 km, the spatial resolution increases to 15 km (the 3.0 GHz channel has a resolution of 25 km), and the radiometric accuracy is 0.5 K. During the operation period of MRM for more than six months in a polar orbit, repeat coverage of brightness temperature (Tb) data at polar regions are obtained. Regarding the sensitivity of passive microwave to the subsurface, the regolith becomes more transparent for longer wavelengths. Therefore, the MRM is able to examine greater depths, and it is feasible to reveal subsurface thermal behavior and regolith thermophysical properties at cold traps (Zheng et al., 2012). Thus, it is necessary to build a microwave radiative transfer model that combines thermal parameters with MRM observations. Here we select Tb data at 37 (Tb_{37}) and 19.35 (Tb_{19}) GHz to retrieve subsurface thermal behavior at cold traps because the two channels are sensitive to temperature variations from surface to ~1 m depth.

In Section 2, we first employed a time- and depth-dependent temperature model. Then the mixture dielectric constant of "wet" regolith (mixed with water ice) was calculated. To derive thermal parameters from high frequency Tb data, a least square method was introduced. Selecting the data sets of Tb_{37} and Tb_{19} covering permanently shaded craters (Cabeus, Haworth and Shoemaker), the attenuation coefficient, thermal gradient and instantaneous temperature profiles were inverted in Section 3. In Section 4, we validated our inversion results and discussed the inversion uncertainty. Finally, we summarized our work and gave the conclusion in Section 5.

2. Method

2.1. Temperature model

Both Apollo 15 and 17 heat flow measurements indicate a low conductivity dust layer that is about 2 cm thick covering the more compacted lunar soil (Keihm et al., 1973). Thus, the one-dimensional thermal model including dust and regolith layers was widely used to investigate regolith thermal behavior from equatorial zone to polar regions (Vasavada et al., 1999, 2012; Paige et al., 2010b). However, it is difficult to accurately simulate subsurface temperature at cold traps because regolith thermophysical properties and interior heat flux are not well constrained, especially at greater depths (> 10 cm) (Paige et al., 2010b).

It is worth noting that although the cold traps are shaded from sunlight, they still are warmed by receiving scattered solar energy, thermal emission from surrounding topography, earthshine and internal heat flux (Vasavada et al., 1999; Paige et al., 2010b). Accordingly, thermal behavior of cold traps also varies as responding to the changes of above heat sources. For example, we collected Tb_{37} data points covering the bottom of Cabeus, Haworth and Shoemaker craters, and found that they still vary with local times in a small but a distinguished fluctuation (as shown in Fig. 1).

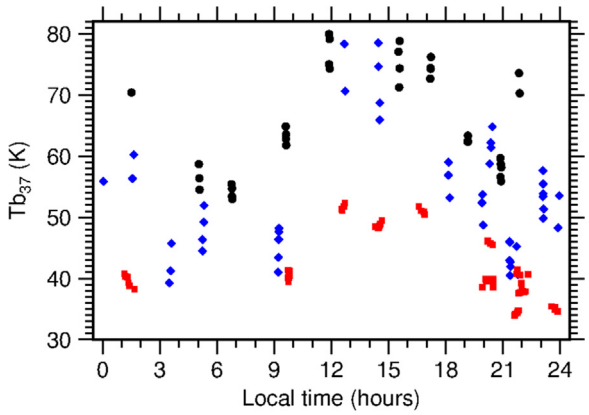

Fig. 1. Tb_{37} at the bottom of different craters varies with local times. The black points, blue diamonds and red squares denote the data covering Cabeus (36°–34.2°W; 84.8°–85°S), Haworth (3°–4.9°W; 86.8°–87°S) and Shoemaker (43.9°–45.9° E; 88.0°–88.2°S), respectively. (For interpretation of the references to color in this figure caption, the reader is referred to the web version of this paper.)

As Tb varies with local time periodically, the time- and depth-dependent temperature can be simulated by Fourier series (Wesselink, 1948; Mezger and Strassl, 1959). Considering heat flux from lunar interior, the temperature model can be written as

$$T(t,z) = T_m + T_a \exp(-\beta z)\cos(\omega t - \beta z) + gz \tag{1}$$

where T_m is mean subsurface temperature, T_a is temperature amplitude, β is attenuation coefficient, ω is angular frequency, t is local time, z is depth, and g is thermal gradient.

2.2. Inversion approach

As indicated by Apollo 17 in situ heat flow measurement, diurnal temperatures decrease drastically with depth in upper layer (< 15 cm) of regolith (Keihm and Langseth, 1973). In order to accurately simulate the temperature profile, we built an inhomogeneous multi-layer model in which the thickness of layer increased with depth exponentially. Thus, more discrete temperature points corresponding to the layers are distributed near the surface. For the nadir viewing of CE-2's MRM (the observation angle equals zero), the contribution of Tb from each layer can be expressed by Eq. (2) based on fluctuation dissipation theory (Jin, 1984; Zhou et al., 2010):

$$Tb_i = \left(1-e^{-2k_i'' d_i}\right)\left(1+|R_{i(i+1)}|^2 e^{-2k_i'' d_i}\right)\prod_{j=0}^{i-1}\left[\left(1-|R_{i(i+1)}|^2\right)e^{-2k_j'' d_j}\right]T_i \tag{2}$$

Additionally, the contribution of Tb from the bottom layer (Tb_n) can be written as (Jin, 1984; Zhou et al., 2010)

$$Tb_n = \prod_{j=0}^{n}\left[\left(1-|R_{j(j+1)}|^2\right)e^{-2k_j'' d_j}\right]T_n \tag{3}$$

Finally, the total contributions of Tb from the multi-layer can be summed up as follows:

$$\begin{aligned} Tb = {} & k_0 \sum_{i=1}^{n-1}\frac{\varepsilon_{ri}''}{2k_{iz}''}\left[1-e^{-2k_{iz}'' d_i}\right] \\ & \cdot\left[1+|R_{i(i+1)}|^2 e^{-2k_{iz}'' d_i}\right]\prod_{j=0}^{i-1}\left[|X_{j(j+1)}|^2 e^{-2k_{iz}'' d_i}\right]T_i \\ & + \frac{k_0 \varepsilon_{rn}''}{2k_{nz}''}|X_{j(j+1)}|^2 e^{-2k_{jz}'' d_j}\prod_{j=0}^{n-1}\left[|X_{j(j+1)}|^2 e^{-2k_{iz}'' d_i}\right]T_n \end{aligned} \tag{4}$$